



## Article

# Full Factorial Design Synthesis of Silver Nanoparticles Using *Origanum vulgare*

Nickolas Rigopoulos <sup>1,\*</sup> , Christina Megetho Gkaliouri <sup>1</sup>, Viktoria Sakavitsi <sup>2</sup> and Dimitrios Gournis <sup>2</sup> 

<sup>1</sup> Department of Food Science and Nutrition, University of the Aegean, Mitropolitou Ioakim 2, Myrina, 81400 Lemnos, Greece; fnsd21008@fns.aegean.gr

<sup>2</sup> Department of Materials Science and Engineering, University of Ioannina, 45110 Ioannina, Greece; viktoriasak@yahoo.gr (V.S.); dgourni@uoi.gr (D.G.)

\* Correspondence: nrigopoulos@aegean.gr

**Abstract:** Green synthesis of silver nanoparticles (AgNPs) involves a reduction reaction of a metal salt solution mixed with a plant extract. The reaction yield can be controlled using several independent factors, such as extract and metal concentration, temperature, and incubation time. AgNPs from *Origanum vulgare* (oregano) were synthesized in the past. However, no investigations were performed on the combined effects of independent factors that affect the synthesis. In this work, silver nitrate, oregano extract, and sodium hydroxide (NaOH) concentrations were chosen as the independent factors, and full factorial design under Response Surface Methodology was employed. UV–Vis absorbance spectroscopy, X-ray Powder Diffraction (XRD), and Fourier Transform Infrared Spectroscopy (FTIR) were used to characterize the nanoparticles. A Voigt function was fitted on the measured UV–Vis spectra. The fitting parameters of the Voigt function, peak wavelength, area, and Full Width at Half Maximum, were used as the responses. A quadratic model was fitted for the peak wavelength and area. The NaOH concentration proved to be the dominant factor in nanoparticle synthesis. UV–Vis absorbance showed a characteristic plasmon resonance of AgNPs at 409 nm. XRD verified the crystallinity of the nanoparticles and FTIR identified the ligands involved.

**Keywords:** silver nanoparticles; green synthesis; full factorial design synthesis; response surface methodology; *Origanum vulgare*



**Citation:** Rigopoulos, N.; Gkaliouri, C.M.; Sakavitsi, V.; Gournis, D. Full Factorial Design Synthesis of Silver Nanoparticles Using *Origanum vulgare*. *Reactions* **2023**, *4*, 505–517. <https://doi.org/10.3390/reactions4030030>

Academic Editors: Annalisa Volpe, Caterina Gaudioso and Maria Chiara Sportelli

Received: 31 July 2023

Revised: 3 September 2023

Accepted: 11 September 2023

Published: 14 September 2023



**Copyright:** © 2023 by the authors. Licensee MDPI, Basel, Switzerland. This article is an open access article distributed under the terms and conditions of the Creative Commons Attribution (CC BY) license (<https://creativecommons.org/licenses/by/4.0/>).

## 1. Introduction

Silver nanoparticles (AgNPs) have demonstrated excellent antimicrobial activities against a variety of microorganisms, which make them suitable for materials used in medical products [1]. Nano-silver has also been used in textiles, coated water filters, for the treatment of mental illness, and other areas [2].

Among various synthesis methods, green synthesis of AgNPs has received attention due to its eco-friendliness, low cost, and capability to integrate microorganisms and biomolecules [3,4]. Silver, gold, and other metallic nanoparticles can be synthesized using plant extracts obtained from dry or fresh leaves, fruits, and seeds [4]. In a typical reaction, a metal salt solution is mixed with the extract, and a reduction in the metal ion occurs [4] with simultaneous capping of the formed nanoparticle [5]. A range of factors control the reaction, such as metal salt and extract concentration, pH, incubation time, and temperature [5,6].

The effects of these different factors can be investigated either by varying ‘one factor at a time’ or by employing the response surface methodology (RSM) that allows studying the effect of several factors simultaneously [7,8]. First- or second-order polynomial equations are adjusted in RSM based on experimental data obtained in an experimental design [8]. Green synthesis of AgNPs based on Gallic Acid (GA) and investigation into the effects of AgNO<sub>3</sub> concentration, GA concentration, and pH were recently performed employing RSM [8]. In another work, temperature, AgNO<sub>3</sub>, and the extract/AgNO<sub>3</sub> ratio were

used as independent factors for nanoparticle synthesis using *Punica granatum* leaves [9]. Two factors, namely  $\text{AgNO}_3$  concentration and pH, were used under RSM for nanoparticle synthesis from the extract of desert truffle *Ascocarps* [10]. Box–Behnken [11] and Plackett–Burman [12] designs under response surface methodology were also used. A full factorial design and a central composite design with four factors, namely incubation time, incubation temperature, dose of the extract, and  $\text{AgNO}_3$  concentration under RSM using *Eucalyptus globulus* fruit were also reported [13]. In contrast, ‘one factor at a time’ was used on AgNP synthesis by *Mentha longifolia* [14].

Oregano (*Origanum vulgare* L.) is an aromatic herb rich in antioxidant compounds including phenolic acids, flavonoids, and essential oils such as thymol, and, as a result, have health benefits for the human body [15]. Origanum-mediated synthesized AgNPs were proposed as alternative antibacterial agents [16,17]. Silver nitrate ( $\text{AgNO}_3$ ) aqueous solutions with concentrations ranging from 0.5 mM to 100 mM are reported [1,17–20] to be used as the precursor for silver ions. The effects of reaction time and temperature were investigated [20].

In this work, the combined effects of incubation time, incubation temperature, metal salt concentration, extract concentration, and sodium hydroxide concentration were investigated using a full factorial design and response surface methodology. The UV–Vis absorption peak wavelength  $\lambda_0$ , the area under the absorption curve (A), and the Full Width at Half Maximum (FWHM) were used as the responses. To our knowledge, this is the first time such work has been reported for AgNPs synthesized using oregano.

## 2. Materials and Methods

### 2.1. Chemicals—Oregano Extract

$\text{AgNO}_3$  aqueous solution (0.1 M) and sodium hydroxide (NaOH) pellets were purchased from Sigma-Aldrich (Steinheim, Germany). Dried oregano (grown on the island of Lemnos) leaves were purchased from a local herb store in Lemnos, Greece.

The oregano extract (OE) was prepared as follows: 3.76 g of dried oregano leaves were boiled in 100 mL distilled water for 10 min. The final extract was obtained with filtering using cheesecloth. The extract was stored at 4 °C for future experiments.

### 2.2. Silver Nanoparticle Synthesis

A final volume of 2.5 mL aqueous solution was used in all syntheses unless otherwise stated.  $\text{AgNO}_3$  ( $C_{\text{AgNO}_3}$ ) (0.25–2 mM) was used as the precursor of silver ions [21]. The reaction started by adding OE at a concentration ( $C_{\text{ext}}$ ) (0.8–20%  $v/v$ ). NaOH ( $C_{\text{NaOH}}$ ) (0–7.9 mM) was also added. In a typical synthesis procedure, a mixture of  $\text{AgNO}_3$ , OE, and NaOH at specific concentrations was heated in a water bath at a temperature (incubation temperature) of 60 °C for 1 h (incubation time). All syntheses was performed in the dark without stirring.

### 2.3. Characterization Techniques

UV–Vis spectroscopy measurements were performed exploiting the Perkin Elmer—Lambda 25 UV–Vis spectrophotometer in the spectral range 340–700 nm, using 1 mL cuvettes with 1 cm path length.

X-ray Diffraction Patterns (XRD) and Fourier Transform Infrared (FTIR) experiments were carried out as described in a previous work [21]. The AgNPs investigated with these techniques (XRD and FTIR) were prepared with the following conditions:  $\text{AgNO}_3$  (1 mM), OE (2%  $v/v$ ), and NaOH (2 mM) were mixed. The obtained nanoparticles were centrifuged at  $20,000 \times g$  for 30 min at 4 °C prior to these measurements.

### 2.4. Statistical Analysis and Experimental Design

As in previous work [21], nanoparticle formation was observed using visual inspection for a color change in the reaction solution and measuring the UV–Vis absorbance of an aliquot. The UV–Vis spectra were fitted using a Voigt profile [22] with fitting pa-

rameters [21]: the peak wavelength ( $\lambda_0$ ) at maximum absorption, the Full Width at Half Maximum (FWHM), and the peak area under the UV–Vis curve (A). The best fit of the UV–Vis absorption spectra was found using the routine Peak Analyzer of the software Origin Pro (version 2020). The quality of fit was determined using the R square regression coefficient ( $R^2 \geq 0.99$ ), and the fit significance was examined using the ANalysis Of Variance (ANOVA) ( $p$ -value smaller than 0.05) [21].

Full Factorial Design (FFD) with three independent factors was applied to the measured UV–Vis spectra: OE concentration ( $X_1$ ),  $\text{AgNO}_3$  concentration ( $X_2$ ), and NaOH concentration ( $X_3$ ). The aim was to investigate the combined effects, if any, of the independent factors on the responses: the peak wavelength ( $\lambda_0$ ), the FWHM, and the peak area (A). Response Surface Methodology (RSM) was employed. Three levels were used for each factor: (−1, 0, and 1). Each of the factors was coded using Equation [23] as follows:

$$X_i = \frac{x_i - x_{oi}}{\Delta x_i}, i = 1, 2, 3 \quad (1)$$

where  $X_i$  and  $x_i$  the coded and the actual value of independent factor  $i$ ,  $x_{oi}$  is the central value (level 0) of factor  $i$ , and  $\Delta x_i$  is the step change in  $x_i$  corresponding to a unit change in the coded value [24].

The central values for the experimental design were  $\text{AgNO}_3$  (1 mM), OE (2%  $v/v$ ), and NaOH (1 mM), with corresponding steps 0.5 mM, 1.2%  $v/v$ , and 1 mM, respectively. A total of 27 runs (Table 1) were conducted in the experiment and the runs were repeated three times each. These factors and their values were selected after preliminary experiments.

**Table 1.** FFD with three synthesis parameters (independent factors) with coded factor levels, actual values into parentheses, and measured three mean responses (wavelength at peak maximum  $\lambda_0$ , peak area A, and FWHM) for AgNPs synthesis via OE.

Run	$X_1$ ( $C_{ext}$ % $v/v$ )	$X_2$ ( $C_{AgNO_3}$ mM)	$X_3$ ( $C_{NaOH}$ mM)	$\lambda_0$ (nm)	Responses A (a.u. *)	FWHM (nm)
1	0 (2)	0 (1)	0 (1)	412.9	129.4	93.7
2	−1 (0.8)	1 (1.5)	1 (2)	405.8	190.5	94.2
3	−1 (0.8)	0 (1)	−1 (0)	439.4	34.7	130.7
4	−1 (0.8)	1 (1.5)	−1 (0)	442.7	31	97.4
5	−1 (0.8)	−1 (0.5)	−1 (0)	438.1	33.5	140.2
6	0 (2)	−1 (0.5)	−1 (0)	441.5	38.5	101.8
7	0 (2)	−1 (0.5)	0 (1)	411.3	63.5	86.4
8	1 (3.2)	1 (1.5)	1 (2)	412.2	214.2	98.6
9	1 (3.2)	1 (1.5)	0 (1)	415.2	170.4	102.4
10	0 (2)	0 (1)	1 (2)	407.5	141.9	93.5
11	−1 (0.8)	−1 (0.5)	0 (1)	407.1	71.9	85.9
12	1 (3.2)	0 (1)	−1 (0)	449.4	97.5	128.9
13	0 (2)	−1 (0.5)	1 (2)	405.2	96.1	112.8
14	0 (2)	1 (1.5)	0 (1)	414.4	147.9	98.5
15	1 (3.2)	0 (1)	1 (2)	409.2	154.1	103.4
16	1 (3.2)	1 (1.5)	−1 (0)	451.1	76.4	106.3
17	0 (2)	0 (1)	−1 (0)	446.1	26.9	84.3
18	1 (3.2)	−1 (0.5)	1 (2)	408.2	92.8	115.9
19	1 (3.2)	−1 (0.5)	0 (1)	411.1	71.6	97.8
20	−1 (0.8)	−1 (0.5)	1 (2)	408.2	97.8	133.7
21	−1 (0.8)	1 (1.5)	0 (1)	412.1	119	95.3
22	1 (3.2)	0 (1)	0 (1)	412.3	145.4	98.9
23	−1 (0.8)	0 (1)	0 (1)	409	106.5	88.4
24	−1 (0.8)	0 (1)	1 (2)	407.6	152.2	102.8
25	0 (2)	1 (1.5)	1 (2)	409.1	194.9	94.2
26	1 (3.2)	−1 (0.5)	−1 (0)	441.1	57.4	97.9
27	0 (2)	1 (1.5)	−1 (0)	450.1	42.1	98.8

\* a.u. = Arbitrary units.

A second-order polynomial was obtained for each response as a function of the coded values ( $X_i$ ) of the independent factors [6,21]:

$$Y_{(response)} = \beta_0 + \sum_i \beta_i X_i + \sum_{i,i} \beta_{i,i} X_i^2 + \sum_{i,j} \beta_{i,j} X_i X_j \quad (2)$$

where  $\beta_0$  denotes the regression coefficient,  $\beta_i$  is the linear coefficient,  $\beta_{ii}$  is the quadratic coefficients,  $\beta_{ij}$  is the second-order interaction coefficients, and  $X_i$  ( $i = 1, 2, 3$ ) is the coded values of the three independent factors [21,25].

Standard procedures were applied to assess the quality of the regression polynomials [23]. ANOVA was applied to assess the significance and adequacy of the model, as well as the significance of the regression coefficients appearing in the derived polynomial [26].

The magnitude and sign of the regression coefficients and Pareto analysis [27] were used as a measure of the importance of the various independent factors and their interactions at a significance level of 5% ( $p$ -value < 0.05), unless otherwise stated. Not statistically significant terms were excluded from the polynomial models except for those required for a hierarchical mode [21].

### 3. Results and Discussion

#### 3.1. UV–Vis Spectra Analysis

An absorption peak within the range of 400–450 nm is indicative of AgNP formation, which is attributed to a surface plasmon resonance [28–30]. Color change in the reaction mixture also allows visual monitoring of AgNP formation [31].

In Figure 1, the combined effects of OE and NaOH concentrations on the UV–Vis spectra are plotted. A better absorption curve can be observed at the lowest extract concentration (OE 2%  $v/v$  Figure 1a) with the presence of NaOH. A Voigt profile was shown to fit adequately with UV–Vis spectra of AgNP solution in a previous study, providing a method of correlation between nanoparticle formation and synthesis parameters [21]. This was the case in this work; however, it occurred only at the lowest extract concentration (OE 2%  $v/v$ ). Agglomerated or ill-formed nanoparticles [32], their crystallinity [33,34], and charge transfer between nanoparticles can influence the observed UV–Vis spectrum [35].

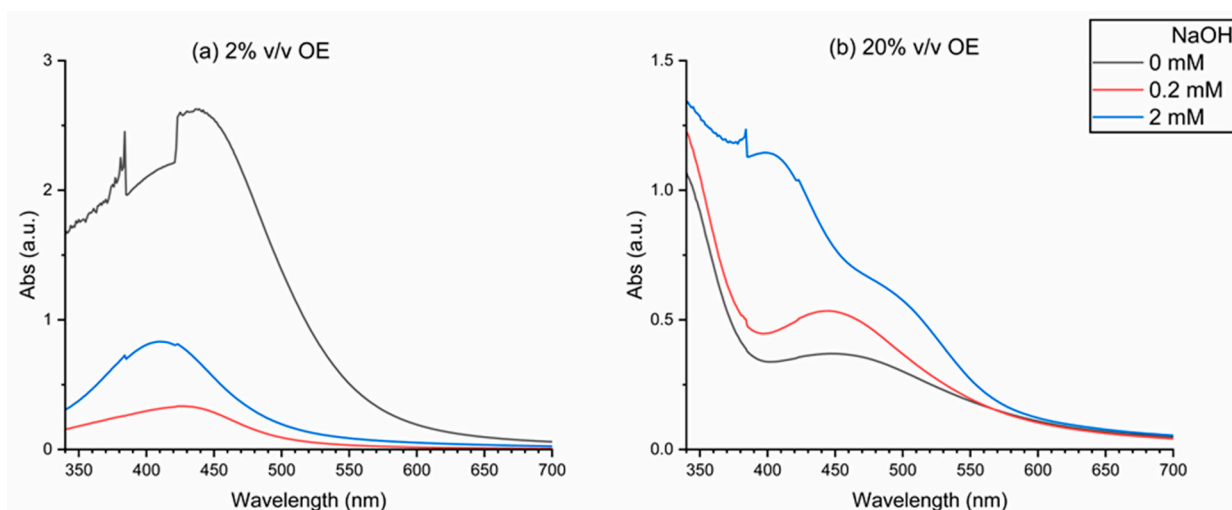


**Figure 1.** Effects of NaOH and OE concentrations on UV–Vis spectra. OE concentration (a) 2%  $v/v$  and (b) 20%  $v/v$ . NaOH concentration: 0, 0.2, and 2 mM.  $\text{AgNO}_3$  concentration, 1 mM; incubation temperature, 40 °C; and incubation time, 10 min.

The addition of NaOH changes the pH of the solution. The pH of the reaction changes the chemical nature of the extract, which has an effect of changing its performance and rate of reduction and therefore nanoparticle synthesis [36]. The size and shape of silver nanoparticles are affected by the pH of the reaction solution [37–40]. This was investigated further

with the addition of hydrochloric acid (HCl), which did not produce any nanoparticles (Figure 2).

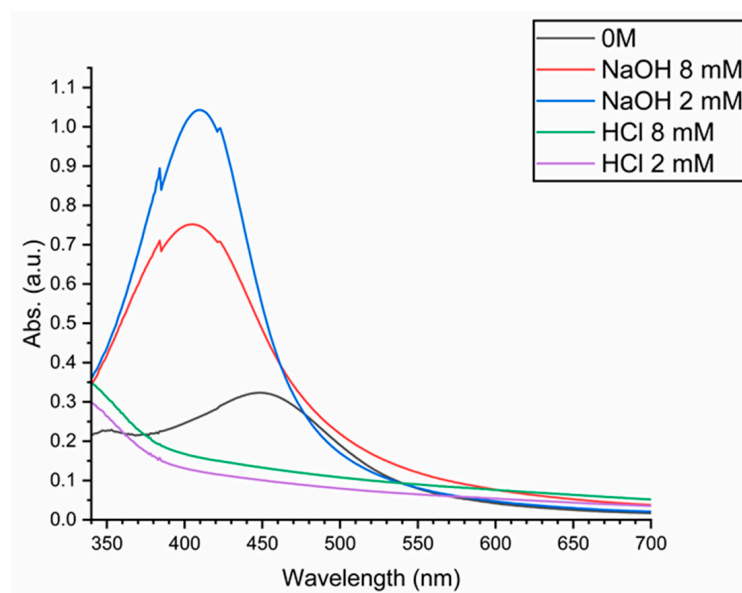


**Figure 2.** Effect of pH on UV–Vis spectra, with the addition of NaOH or HCl at different concentrations. AgNO<sub>3</sub> concentration, 1 mM; OE concentration, 2% *v/v*; incubation temperature, 60 °C; and incubation time, 1 h.

The fitting parameters used in the Voigt profile are related to nanoparticle size, shape, yield, and size distribution [21]. It was an attempt to determine the appropriate conditions that produce the smallest peak wavelength with maximum peak area and narrowest FWHM. From the findings, the smallest peak was achieved at incubation temperature (60 °C), incubation time 1 h, and NaOH (0–2 mM) (Supporting Information: Figures S1 and S3; Tables S1 and S2).

The corresponding ranges of OE and AgNO<sub>3</sub> concentrations were investigated in a similar manner as shown in Figure 3. The investigation (see Supporting Information: Table S3) determined a range (0.5–1.5 mM) for AgNO<sub>3</sub> and (0.8–3.2% *v/v*) for OE concentrations.

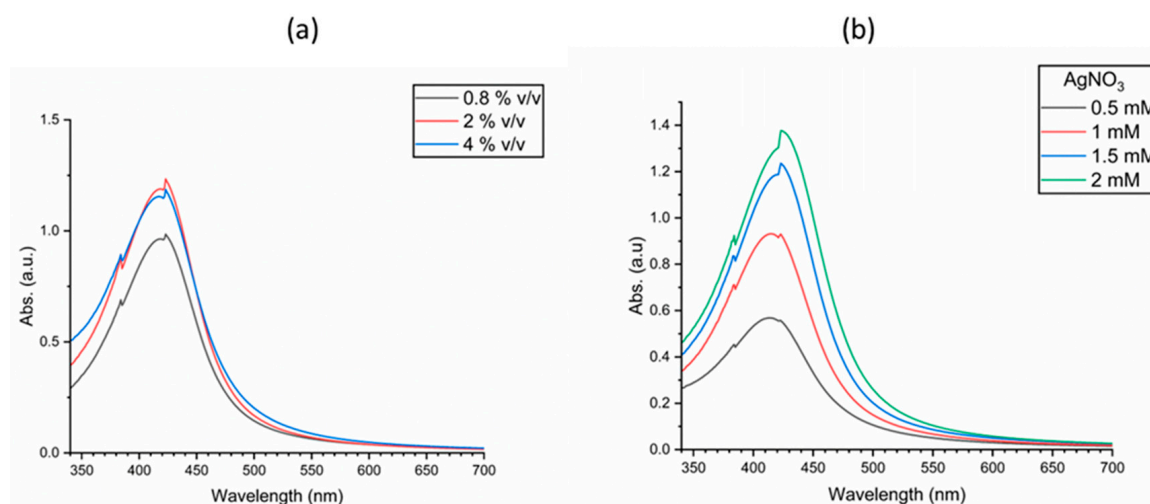


**Figure 3.** Effect of (a) OE extract concentration (with AgNO<sub>3</sub> 1 mM), and (b) AgNO<sub>3</sub> concentration (with OE 2% *v/v*) on UV–Vis spectra. NaOH concentration 1 mM; incubation temperature 60 °C; and incubation time 1 h.

### 3.2. Statistical Modeling of AgNP Synthesis

A quadratic regression model (Equation (2)) was applied for each response in order to better understand the effect of all independent factors as well as their interactions in the AgNPs synthesis. The ANOVA for each response is given in Tables 2–4.

**Table 2.** ANOVA for the quadratic model for wavelength at peak maximum  $\lambda_0$ .

Source	df	SS	MS	F *	p-Value
Model	9	22,322.92	2480.32	138.19	<0.0001
Linear					
$X_1$	1	264.48	264.48	14.74	
$X_2$	1	278.24	278.24	15.50	
$X_3$	1	17,798.83	17,798.83	991.68	
Square					
$X_3^2$	1	3813.3	3813.3	212.46	
Interaction					
$X_2X_3$	1	77.74	77.74	4.33	
Error	71	1274.32	17.95		
Lack of fit	17	117.17	6.89	0.3217	
Pure error	54	1157.15	21.43		
Total	80	23,597.24			

df = degrees of freedom, SS = Sum of Squares, MS = Mean Square, \* F statistic.

**Table 3.** ANOVA for the quadratic model for peak area A.

Source	df	SS	MS	F *	p-Value
Model	9	231,000	25,662.02	76.05	<0.0001
Linear					
$X_1$	1	9827.11	9827.11	29.12	
$X_2$	1	52,886.07	52,886.07	156.73	
$X_3$	1	133,900	133,900	396.83	
Square					
$X_2^2$	1	1556.99	1556.99	4.61	
$X_3^2$	1	4321.69	4321.69	12.81	
Interaction					
$X_1X_2$	1	2595.25	2595.25	7.69	
$X_1X_3$	1	3111.7	3111.7	9.22	
$X_2X_3$	1	21,421.51	21,421.51	63.48	
Error	71	23,958.08	337.44		
Lack of fit	17	6523.82	383.75	1.19	
Pure error	54	17,434.25	322.86		
Total	80	254,900			

Df = degrees of freedom, SS = Sum of Squares, MS = Mean Square, \* F statistic.

**Table 4.** ANOVA for quadratic model for FWHM.

Source	df	SS	MS	* F	p-Value
Model	9	8440.95	937.88	1.56	0.1435
Linear					
$X_3$	1	230.88	230.88	0.3847	
Square					
$X_3^2$	1	3220.51	3220.51	5.37	
Error	71	42,616.33	600.23		
Lack of fit	17	8700.41	511.79	0.8149	
Pure error	54	33,915.92	628.07		
Total	80	51,057.28			

df = degrees of freedom, SS = Sum of Squares, MS = Mean Square, \* F statistic.



A  $p$ -value smaller than 0.001 can be observed for the quadratic model for both the peak wavelength at maximum  $\lambda_0$  (Table 2) and the peak area A (Table 3), indicating that the quadratic model was suitable for both responses. This is further supported by the large value of the F statistic. In contrast, a pure model can be observed for the FWHM (Table 4) ( $p$ -value = 0.1435) and  $F = 1.56$ . The coefficient of determination ( $R^2$ ) of the models for the peak wavelength was 93.92%, whereas for the peak area was 89.41%, which indicated a significant correlation between the observed and predicted values [6,23,41]. The model adequacy was tested by applying standard diagnostic tools (see Supplementary Material) [23,26].

The regression coefficients for the wavelength at peak maximum  $\lambda_0$  are given in Table 5. The wavelength is affected mainly by the NaOH concentration ( $X_3$ ), followed by equal contribution from OE ( $X_1$ ) and  $\text{AgNO}_3$  ( $X_2$ ) concentrations. A large contribution appears from the quadratic term of NaOH concentration. A small contribution also appears from the interaction term  $X_2X_3$  of  $\text{AgNO}_3$  and NaOH concentrations. Terms where NaOH concentration appears contribute negatively to the peak wavelength.

**Table 5.** Regression coefficients for wavelength at peak maximum  $\lambda_0$ .

Model Term	CE	Std. Error
Intercept	412.4	1.25
$X_1$	2.21	0.5765
$X_2$	2.27	0.5765
$X_3$	−18.16	0.5765
$X_2X_3$	−1.47	0.7061
$X_3^2$	14.56	0.9986

CE = Coefficient Estimate, Std. Error = Standard Error,  $R^2 = 93.92\%$ .

The response surface (peak wavelength) for AgNP synthesis therefore is provided by the following second-order polynomial:

$$Y_{(\text{peak wavelength})} = 412.4 + 2.21X_1 + 2.27X_2 - 18.16X_3 - 1.47X_2X_3 + 14.56X_3^2 \quad (3)$$

The regression coefficients for peak area A are given in Table 6. The area is affected almost equally by NaOH ( $X_3$ ) and  $\text{AgNO}_3$  ( $X_2$ ) concentrations, followed by the OE ( $X_1$ ) concentration. A large contribution appears from the interaction term  $X_2X_3$  of  $\text{AgNO}_3$  and NaOH concentrations, followed by a smaller contribution from the interaction terms  $X_1X_2$  of OE and  $\text{AgNO}_3$  concentrations, and the interaction  $X_1X_3$  with the negative sign of OE and NaOH concentrations. A large negative contribution appears for the quadratic terms of both  $\text{AgNO}_3$  and NaOH concentrations.

**Table 6.** Regression coefficients for peak area A.

Model Term	CE	Std. Error
Intercept	114.44	5.40
$X_1$	13.49	2.5
$X_2$	31.29	2.5
$X_3$	49.80	2.5
$X_1X_2$	8.49	2.39
$X_1X_3$	−9.30	−15.40
$X_2X_3$	24.39	18.29
$X_2^2$	−9.30	−17.93
$X_3^2$	−15.49	−24.13

CE = Coefficient Estimate, Std. Error = Standard Error,  $R^2 = 89.41\%$ .

The response surface (peak area) for AgNPs synthesis therefore is provided by the following second-order polynomial:

$$Y_{(peak\ area)} = 114.44 + 13.49X_1 + 31.29X_2 + 49.8X_3 + 8.49X_1X_2 - 9.3X_1X_3 + 24.39X_2X_3 - 9.3X_2^2 - 15.49X_3^2 \quad (4)$$

Pareto analysis percentages are shown in Table 7 for the wavelength at peak maximum  $\lambda_0$  and the peak area A quadratic model terms. In both cases, the largest contribution comes from the NaOH concentration ( $X_3$ ) with values of 59.53% (wavelength) and 52.53% (area). A total of 97.8% of the peak wavelength is influenced by the linear and quadratic term of NaOH concentration, in contrast to 57.61% for the peak area. The peak area is correlated to the quantity of formed nanoparticles, which should depend on both  $\text{AgNO}_3$  (20.74%) and OE concentrations (3.85%). This is not sufficient, however, for the synthesis of nanoparticles, as the presence of NaOH plays a crucial role in both the number of formed nanoparticles (area) and their size (wavelength). This agrees with previous work reporting the effect of pH on nanoparticle size [36,38,40]. A total of 96.9% contribution from the linear term of pH on nanoparticle size was reported on green synthesis of silver nanoparticles from gallic acid [8]. In contrast, in a previous work [21], the linear term of pH contributes only 10% to the peak wavelength, with the largest contribution (59%) from the third-order interaction term ( $BPE^2 \times pH$ ) (BPE = Banana Peel Extract concentration, see Supporting Information Table S4). The observed different contributions of pH from different plant extracts can be attributed to different compounds involved in metal salt reduction and nanoparticle formation.

**Table 7.** Pareto analysis [27] for significant terms in the quadratic model for both the peak wavelength  $\lambda_0$  and peak area A.

Peak Wavelength $\lambda_0$		Peak Area A	
Term	Per. Ef (%)	Term	Per. Ef (%)
$X_1$	0.88	$X_1$	3.85
$X_2$	0.93	$X_2$	20.74
$X_3$	59.53	$X_3$	52.53
$X_2X_3$	0.39	$X_1X_2$	1.53
$X_3^2$	38.27	$X_1X_3$	1.83
-	-	$X_2X_3$	12.6
-	-	$X_2^2$	1.83
-	-	$X_3^2$	5.08

Per. Ef = Percentage effect.

Examination of the data (Table 1) revealed that the best UV–Vis spectra in terms of minimum wavelength  $\lambda_0$  at peak maximum, minimum FWHM, and maximum area A can be obtained for the factor combination corresponding to experimental run 23. This run corresponds to an actual OE concentration of 0.8% *v/v*,  $\text{AgNO}_3$  concentration of 1 mM, and NaOH concentration of 1 mM. The measured peak wavelength of 409 nm is smaller than the values reported by other groups [1,17–20] who have not investigated pH effects.

### 3.3. XRD

The XRD pattern of the dry powder obtained from the formed AgNPs synthesized using oregano revealed the amorphous nature of the sample, as evidenced by a broad peak at  $\sim 25^\circ$ . This peak is possibly due to the oregano, although there are discernible Ag contributions from the AgNPs, which overlap with this broad pattern. This behavior is rational since the characteristic peaks of AgNPs are, in general, not easily recognizable when synthesized using natural products. However, in our case the more intense peaks of AgNPs corresponding to (111), (200), (220), and (311) reflections are still visible at  $38.14^\circ$ ,  $43.69^\circ$ ,  $64.24^\circ$ , and  $77.40^\circ$ , respectively (Figure 4), indicating the successful formation of silver nanoparticles [21,42–48].



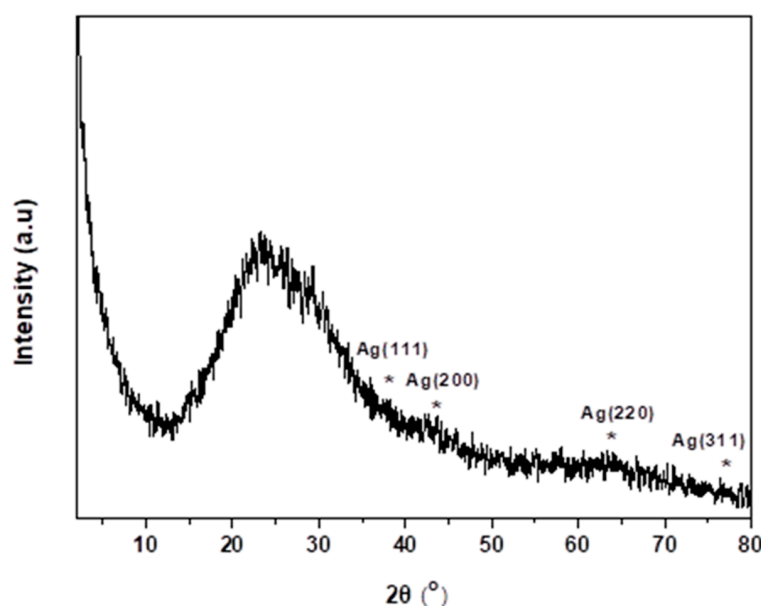


**Figure 4.** X-ray diffraction pattern of AgNPs, with hkl Ag peaks.

### 3.4. FTIR

FTIR was used to identify the ligands that surround the nanoparticle surface. Seven absorption bands appear in the spectrum (Figure 5). The weak band at  $3749\text{ cm}^{-1}$  indicates the presence of polyphenols due to the binding of silver ions with hydroxyl group [21,49]. The band at  $3438\text{ cm}^{-1}$  originates either from O-H or NH stretching vibration [50,51]. The band at  $2963\text{ cm}^{-1}$  indicates C-H stretching for an alkane [52]. The small shoulder formed at  $2850\text{ cm}^{-1}$  and  $2918\text{ cm}^{-1}$  arises from the C-H stretching vibrations either from -C-H- or -C-H<sub>2</sub>-aliphatic compounds [50,51]. The band at  $1633\text{ cm}^{-1}$  is attributed to the C-N and C-C stretching [21,49]. The sharp band at  $1384\text{ cm}^{-1}$  corresponds to the N=O symmetry stretching, typical of the nitro compounds [21,49]. The bands at  $1060\text{ cm}^{-1}$  and  $1112\text{ cm}^{-1}$  are assigned to stretching vibration C-O [53]. The band around  $836\text{ cm}^{-1}$  could be attributed to out-of-plane C-H wagging vibrations, the most significant signal used in distinguishing between different types of aromatic ring substitution [54].

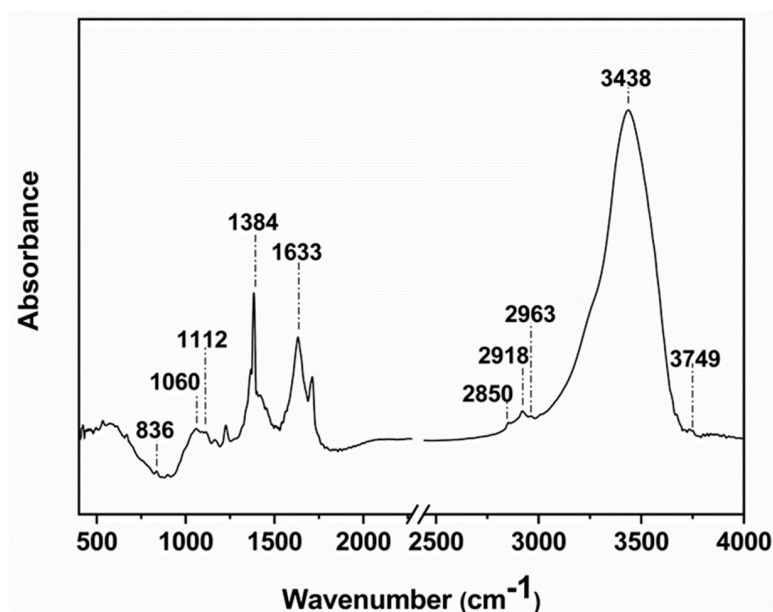


**Figure 5.** FTIR spectrum of AgNPs synthesized using oregano extract.

#### 4. Conclusions

Silver nanoparticles were synthesized using oregano extract. The synthesis can be affected by parameters such as metal salt concentration, oregano extract concentration, NaOH concentration, incubation time, and temperature. The combined effects of silver nitrate concentration, oregano concentration, and NaOH concentration were investigated using Full Factorial Design under Response Surface Methodology. These concentrations were the independent factors.

A Voigt function could be fitted on the UV–Vis spectra, with parameters the wavelength at peak maximum  $\lambda_0$ , the peak area  $A$  under the curve, and the Full Width at Half Maximum. These three parameters were chosen as the responses. A quadratic model could be fitted on both the wavelength  $\lambda_0$  and the area  $A$ .

The investigation showed that the NaOH concentration or equivalent to the pH of the solution, is the main factor that influences the nanoparticle synthesis, both in terms of size and quantity. The proposed model opens the possibility for size tuning of silver nanoparticles synthesized using oregano extract. Size determines the surface/volume ratio of a nanoparticle, which in turn can alter the interaction of the nanoparticle with the surrounding environment. This opens up the possibility for improved nanoparticle properties for specific applications.

**Supplementary Materials:** The following supporting information can be downloaded at <https://www.mdpi.com/article/10.3390/reactions4030030/s1>. Figure S1: Effect of incubation temperature on UV–Vis spectra: (a) 40 °C, (b) 60 °C. AgNO<sub>3</sub> concentration 1 mM, OE concentration 2% v/v, NaOH concentration 2 mM, and incubation time 10 min; Figure S2: Effect of incubation time on UV–Vis spectra. AgNO<sub>3</sub> concentration 1 mM, OE concentration 2% v/v, NaOH concentration 2 mM, and incubation temperature 60 °C; Figure S3: Effect of NaOH or HCl concentration on UV–Vis spectra. (a) Coarse investigation, (b) fine tuning. AgNO<sub>3</sub> concentration 1 mM, OE concentration 2% v/v, incubation temperature 60 °C, and incubation time 1 h; Figure S4: Normal probability plot of residuals: (a) wavelength at peak maximum  $\lambda_0$ , and (b) peak area  $A$ ; Table S1: Fitting parameters of a Voigt function ( $\lambda_0$ ,  $A$ , and FWHM) discussed in the text for UV–Vis spectra at different incubation temperatures and times. AgNO<sub>3</sub> concentration 1 mM, OE concentration 2% v/v, and NaOH concentration 2 mM; Table S2: Fitting parameters of a Voigt function ( $\lambda_0$ ,  $A$ , and FWHM) discussed in the text, for UV–Vis spectra at different NaOH concentrations. AgNO<sub>3</sub> concentration 1 mM, OE concentration 2% v/v, incubation temperature 60 °C, and incubation time; Table S3: Fitting parameters of a Voigt function ( $\lambda_0$ ,  $A$ , and FWHM) discussed in the text, for UV–Vis spectra at different OE and AgNO<sub>3</sub> concentrations. NaOH concentration 1 mM, incubation temperature 60 °C, and incubation time 1 h; Table S4: Pareto analysis for significant terms ( $p$ -value < 0.05) in the quadratic model for particle size, and the cubic model for the peak wavelength  $\lambda_0$ .

**Author Contributions:** Conceptualization, N.R.; Data curation, N.R., C.M.G. and V.S.; Formal analysis, N.R. and D.G.; Investigation, N.R., C.M.G., V.S. and D.G.; Methodology, N.R. and D.G.; Project N.R., V.S. and D.G.; Funding acquisition, D.G.; Administration, N.R.; Resources, D.G.; Software, N.R., C.M.G. and V.S.; Supervision, N.R. and D.G.; Validation, N.R., V.S. and D.G.; Visualization, N.R.; Writing—original draft, N.R., C.M.G. and V.S.; Writing—review and editing, N.R., C.M.G., V.S. and D.G. All authors have read and agreed to the published version of the manuscript.

**Funding:** This research received no external funding.

**Data Availability Statement:** The data presented in this study are available on request from the corresponding author.

**Acknowledgments:** Nickolas Rigopoulos and Chrisitna Megetho Gkaliouri would like to acknowledge the valuable technical support of Andreas Petsas from the Department of Food Science and Nutrition, University of the Aegean.

**Conflicts of Interest:** The authors declare no conflict of interest. The authors have no competing interests to declare that are relevant to the content of this article. All authors certify that they have no affiliations with or involvement in any organization or entity with any financial interest or non-financial interest in the subject matter or materials discussed in this manuscript. The authors have no financial or proprietary interests in any material discussed in this article. The datasets generated during and/or analyzed during the current study are available from the corresponding author upon reasonable request. The funders had no role in the design of the study; in the collection, analyses, or interpretation of data; in the writing of the manuscript; or in the decision to publish the results.

## References

1. Shaik, M.R.; Khan, M.; Kuniyil, M.; Al-Warthan, A.; Alkhathlan, H.Z.; Siddiqui, M.R.H.; Shaik, J.P.; Ahamed, A.; Mahmood, A.; Khan, M.; et al. Plant-Extract-Assisted Green Synthesis of Silver Nanoparticles Using *Origanum vulgare* L. Extract and Their Microbicidal Activities. *Sustainability* **2018**, *10*, 913. [\[CrossRef\]](#)
2. Galatage, S.T.; Hebalkar, A.S.; Dhobale, S.V.; Mali, O.R.; Kumbhar, P.S.; Nikade, S.V.; Killedar, S.G. Silver Nanoparticles: Properties, Synthesis, Characterization, Applications and Future Trends. In *Silver Micro-Nanoparticles—Properties, Synthesis, Characterization, and Applications*; IntechOpen: London, UK, 2021. [\[CrossRef\]](#)
3. Roy, S.; Rhim, J.W. Starch/Agar-Based Functional Films Integrated with Enoki Mushroom-Mediated Silver Nanoparticles for Active Packaging Applications. *Food Biosci.* **2022**, *49*, 101867. [\[CrossRef\]](#)
4. Saravanan, A.; Kumar, P.S.; Hemavathy, R.V.; Jeevanantham, S.; Jawahar, M.J.; Neshaanthini, J.P.; Saravanan, R. A Review on Synthesis Methods and Recent Applications of Nanomaterial in Wastewater Treatment: Challenges and Future Perspectives. *Chemosphere* **2022**, *307*, 135713. [\[CrossRef\]](#) [\[PubMed\]](#)
5. Sharma, K.; Guleria, S.; Salaria, K.H.; Majeed, A.; Sharma, N.; Pawar, K.D.; Thakur, V.K.; Gupta, V.K. Photocatalytic and Biological Properties of Silver Nanoparticles Synthesized Using Callistemon Lanceolatus Leaf Extract. *Ind. Crops Prod.* **2023**, *202*, 116951. [\[CrossRef\]](#)
6. Barabadi, H.; Honary, S.; Ebrahimi, P.; Alizadeh, A.; Naghibi, F.; Saravanan, M. Optimization of Myco-Synthesized Silver Nanoparticles by Response Surface Methodology Employing Box-Behnken Design. *Inorg. Nano-Met. Chem.* **2019**, *49*, 33–43. [\[CrossRef\]](#)
7. Balachandran, M.; Devanathan, S.; Muraleekrishnan, R.; Bhagawan, S.S. Optimizing Properties of Nanoclay-Nitrile Rubber (NBR) Composites Using Face Centred Central Composite Design. *Mater. Des.* **2012**, *35*, 854–862. [\[CrossRef\]](#)
8. Ahani, M.; Khatibzadeh, M. Size Optimisation of Silver Nanoparticles Synthesised by Gallic Acid Using the Response Surface Methodology. *Micro Nano Lett.* **2020**, *15*, 403–408. [\[CrossRef\]](#)
9. Singhal, M.; Chatterjee, S.; Kumar, A.; Syed, A.; Bahkali, A.H.; Gupta, N.; Nimesh, S. Exploring the Antibacterial and Antibiofilm Efficacy of Silver Nanoparticles Biosynthesized Using Punica Granatum Leaves. *Molecules* **2021**, *26*, 5762. [\[CrossRef\]](#)
10. Alshammari, S.O.; Abd El Aty, A.A. Statically Controlled Mycogenic-Synthesis of Novel Biologically Active Silver-Nanoparticles Using Hafr Al-Batin Desert Truffles and Its Antimicrobial Efficacy against Pathogens. *Saudi J. Biol. Sci.* **2022**, *29*, 103334. [\[CrossRef\]](#)
11. Kujur, A.; Daharwal, S.J. Box–Behnken Design Based Optimization of Process Variables for the Green Synthesis of 18-Beta-Glycyrrhetic Acid Silver Nanoparticles and Evaluation of Its Antioxidant, Antimicrobial Activity. *Int. J. Drug Deliv. Technol.* **2023**, *13*, 501–509. [\[CrossRef\]](#)
12. Naysmith, A.; Mian, N.S.; Rana, S. Development of Conductive Textile Fabric Using Plackett–Burman Optimized Green Synthesized Silver Nanoparticles and in Situ Polymerized Polypyrrole. *Green Chem. Lett. Rev.* **2023**, *16*, 2158690. [\[CrossRef\]](#)
13. Sarkar, M.; Denrah, S.; Das, M.; Das, M. Statistical Optimization of Bio-Mediated Silver Nanoparticles Synthesis for Use in Catalytic Degradation of Some Azo Dyes. *Chem. Phys. Impact* **2021**, *3*, 100053. [\[CrossRef\]](#)
14. Javed, B.; Nadhman, A.; Mashwani, Z.U.R. Optimization, Characterization and Antimicrobial Activity of Silver Nanoparticles against Plant Bacterial Pathogens Phyto-Synthesized by Mentha Longifolia. *Mater. Res. Express* **2020**, *7*, 085406. [\[CrossRef\]](#)
15. Mikołajczak, A.; Ligaj, M.; Kobus-Cisowska, J. Temperature Optimization by Electrochemical Method for Improving Antioxidant Compound Extraction Efficiency from *Origanum vulgare* L. and Its Application in a Bread Production. *Sustainability* **2022**, *14*, 2801. [\[CrossRef\]](#)
16. Hambardzumyan, S.; Sahakyan, N.; Petrosyan, M.; Nasim, M.J.; Jacob, C.; Trchounian, A. *Origanum vulgare* L. Extract-Mediated Synthesis of Silver Nanoparticles, Their Characterization and Antibacterial Activities. *AMB Express* **2020**, *10*, 162. [\[CrossRef\]](#)
17. Sankar, R.; Karthik, A.; Prabu, A.; Karthik, S.; Shivashangari, K.S.; Ravikumar, V. Origanum Vulgare Mediated Biosynthesis of Silver Nanoparticles for Its Antibacterial and Anticancer Activity. *Colloids Surf. B Biointerfaces* **2013**, *108*, 80–84. [\[CrossRef\]](#)
18. Baláž, M.; Balážová, L.; Daneu, N.; Dutková, E.; Balážová, M.; Bujňáková, Z.; Shpotyuk, Y. Plant-Mediated Synthesis of Silver Nanoparticles and Their Stabilization by Wet Stirred Media Milling. *Nanoscale Res. Lett.* **2017**, *12*, 83. [\[CrossRef\]](#)
19. Baláž, M.; Balážová, L.; Kováčová, M.; Daneu, N.; Salayová, A.; Bedlovičová, Z.; Tkáčiková, L. The Relationship between Precursor Concentration and Antibacterial Activity of Biosynthesized Ag Nanoparticles. *Adv. Nano Res.* **2019**, *7*, 125–134. [\[CrossRef\]](#)
20. Salayová, A.; Bedlovičová, Z.; Daneu, N.; Baláž, M.; Lukáčová Bujňáková, Z.; Balážová, L.; Tkáčiková, L. Green Synthesis of Silver Nanoparticles with Antibacterial Activity Using Various Medicinal Plant Extracts: Morphology and Antibacterial Efficacy. *Nanomaterials* **2021**, *11*, 1005. [\[CrossRef\]](#)

21. Rigopoulos, N.; Thomou, E.; Kouloumpis, A.; Lamprou, E.R.; Petropoulea, V.; Gournis, D.; Poulis, E.; Karantonis, H.C.; Giaouris, E. Optimization of Silver Nanoparticle Synthesis by Banana Peel Extract Using Statistical Experimental Design, and Testing of Their Antibacterial and Antioxidant Properties. *Curr. Pharm. Biotechnol.* **2019**, *20*, 858–873. [\[CrossRef\]](#)
22. Belafhal, A. Shape of Spectral Lines: Widths and Equivalent Widths of the Voigt Profile. *Opt. Commun.* **2000**, *177*, 111–118. [\[CrossRef\]](#)
23. El-Naggar, N.E.A.; Abdelwahed, N.A.M. Application of Statistical Experimental Design for Optimization of Silver Nanoparticles Biosynthesis by a Nanofactory *Streptomyces Viridochromogenes*. *J. Microbiol.* **2014**, *52*, 53–63. [\[CrossRef\]](#) [\[PubMed\]](#)
24. Karvela, E.; Makris, D.P.; Kalogeropoulos, N.; Karathanos, V.T. Deployment of Response Surface Methodology to Optimise Recovery of Grape (*Vitis Vinifera*) Stem Polyphenols. *Talanta* **2009**, *79*, 1311–1321. [\[CrossRef\]](#) [\[PubMed\]](#)
25. Biswas, S.; Mulaba-Bafubandi, A.F. Optimization of Process Variables for the Biosynthesis of Silver Nanoparticles by *Aspergillus Wentii* Using Statistical Experimental Design. *Adv. Nat. Sci. Nanosci. Nanotechnol.* **2016**, *7*, 045005. [\[CrossRef\]](#)
26. Montgomery, D.C. *Design and Analysis of Experiments*, 8th ed.; John Wiley & Sons: Hoboken, NJ, USA, 2013.
27. Asadzadeh, F.; Maleki-Kaklar, M.; Soiltanalinejad, N.; Shabani, F. Central Composite Design Optimization of Zinc Removal from Contaminated Soil, Using Citric Acid as Biodegradable Chelant. *Sci. Rep.* **2018**, *8*, 2633. [\[CrossRef\]](#)
28. Amendola, V.; Bakr, O.M.; Stellacci, F. A Study of the Surface Plasmon Resonance of Silver Nanoparticles by the Discrete Dipole Approximation Method: Effect of Shape, Size, Structure, and Assembly. *Plasmonics* **2010**, *5*, 85–97. [\[CrossRef\]](#)
29. Bindhu, M.R.; Umadevi, M. Synthesis of Monodispersed Silver Nanoparticles Using Hibiscus Cannabinus Leaf Extract and Its Antimicrobial Activity. *Spectrochim. Acta Part A Mol. Biomol. Spectrosc.* **2013**, *101*, 184–190. [\[CrossRef\]](#)
30. Basiuk, V.A.; Basiuk, E.V. *Green Processes for Nanotechnology: From Inorganic to Bioinspired Nanomaterials*; Springer International Publishing: Cham, Switzerland, 2015; pp. 1–446. [\[CrossRef\]](#)
31. Ibrahim, H.M.M. Green Synthesis and Characterization of Silver Nanoparticles Using Banana Peel Extract and Their Antimicrobial Activity against Representative Microorganisms. *J. Radiat. Res. Appl. Sci.* **2015**, *8*, 265–275. [\[CrossRef\]](#)
32. Valenti, L.E.; Giacomelli, C.E. Stability of Silver Nanoparticles: Agglomeration and Oxidation in Biological Relevant Conditions. *J. Nanoparticle Res.* **2017**, *19*, 858–873. [\[CrossRef\]](#)
33. Molleman, B.; Hiemstra, T. Surface Structure of Silver Nanoparticles as a Model for Understanding the Oxidative Dissolution of Silver Ions. *Langmuir* **2015**, *31*, 13361–13372. [\[CrossRef\]](#)
34. Khan, M.A.M.; Kumar, S.; Ahamed, M.; Alrokayan, S.A.; AlSalhi, M.S. Structural and Thermal Studies of Silver Nanoparticles and Electrical Transport Study of Their Thin Films. *Nanoscale Res. Lett.* **2011**, *6*, 434. [\[CrossRef\]](#) [\[PubMed\]](#)
35. Quinten, M. *Optical Properties of Nanoparticle Systems*; Wiley—Vch Verlag GmbH & Co. KGaA: Weinheim, Germany, 2011. [\[CrossRef\]](#)
36. Dada, A.O.; Adekola, F.A.; Adeyemi, O.S.; Bello, O.M.; Oluwaseun, A.C.; Awakan, O.J.; Grace, F.-A.A. Exploring the Effect of Operational Factors and Characterization Imperative to the Synthesis of Silver Nanoparticles. In *Silver Nanoparticles—Fabrication, Characterization and Applications*; InTech: London, UK, 2018. [\[CrossRef\]](#)
37. Roustia, M.H.; Ghasemi, N. Green Synthesis of Silver Nanoparticles Using a Mountain Plant Extract. *Rev. Roum. Chim.* **2019**, *64*, 143–152. [\[CrossRef\]](#)
38. Marciniak, L.; Nowak, M.; Trojanowska, A.; Tylkowski, B.; Jastrzab, R. The Effect of Ph on the Size of Silver Nanoparticles Obtained in the Reduction Reaction with Citric and Malic Acids. *Materials* **2020**, *13*, 5444. [\[CrossRef\]](#) [\[PubMed\]](#)
39. Handayani, W.; Ningrum, A.S.; Imawan, C. The Role of PH in Synthesis Silver Nanoparticles Using Pometia Pinnata (Matoa) Leaves Extract as Bioreductor. *J. Phys. Conf. Ser.* **2020**, *1428*, 012021. [\[CrossRef\]](#)
40. Alqadi, M.K.; Abo Noqtah, O.A.; Alzoubi, F.Y.; Aljarrah, K. PH Effect on the Aggregation of Silver Nanoparticles Synthesized by Chemical Reduction. *Mater. Sci. Pol.* **2014**, *32*, 107–111. [\[CrossRef\]](#)
41. Kaushik, R.; Saran, S.; Isar, J.; Saxena, R.K. Statistical Optimization of Medium Components and Growth Conditions by Response Surface Methodology to Enhance Lipase Production by *Aspergillus Carneus*. *J. Mol. Catal. B Enzym.* **2006**, *40*, 121–126. [\[CrossRef\]](#)
42. Supraja, N.; Prasad, T.N.V.K.V.; Soundariya, M.; Babujanathanam, R. Synthesis, Characterization and Dose Dependent Antimicrobial and Anti-Cancerous Activity of Phycogenic Silver Nanoparticles against Human Hepatic Carcinoma (HepG2) Cell Line. *AIMS Bioeng* **2016**, *3*, 425–440. [\[CrossRef\]](#)
43. Umadevi, M.; Shalini, S.; Bindhu, M.R. Synthesis of Silver Nanoparticle Using D. Carota Extract. *Adv. Nat. Sci. Nanosci. Nanotechnol.* **2012**, *3*, 025008. [\[CrossRef\]](#)
44. Raut Rajesh, W.; Lakkakula Jaya, R.; Kolekar Niranjana, S.; Mendhulkar Vijay, D.; Kashid Sahebrao, B. Phytosynthesis of Silver Nanoparticle Using *Gliricidia Sepium* (Jacq.). *Curr. Nanosci.* **2009**, *5*, 117–122. [\[CrossRef\]](#)
45. Pavani, K.V.; Gayathamma, K.; Banerjee, A.; Suresh, S. Phyto-Synthesis of Silver Nanoparticles Using Extracts of *Ipomoea indica* Flowers. *Am. J. Nanomater.* **2013**, *1*, 5–8. [\[CrossRef\]](#)
46. Al-Khedhairi, A.A.; Wahab, R. Silver Nanoparticles: An Instantaneous Solution for Anticancer Activity against Human Liver (HepG2) and Breast (MCF-7) Cancer Cells. *Metals* **2022**, *12*, 148. [\[CrossRef\]](#)
47. Shameli, K.; Ahmad, M.B.; Zamanian, A.; Sangpour, P.; Shabanzadeh, P.; Abdollahi, Y.; Zargar, M. Green Biosynthesis of Silver Nanoparticles Using Curcuma Longa Tuber Powder. *Int. J. Nanomed.* **2012**, *7*, 5603–5610. [\[CrossRef\]](#) [\[PubMed\]](#)
48. Vanaja, M.; Annadurai, G. Coleus Aromaticus Leaf Extract Mediated Synthesis of Silver Nanoparticles and Its Bactericidal Activity. *Appl. Nanosci.* **2013**, *3*, 217–223. [\[CrossRef\]](#)

49. Mohanta, Y.K.; Panda, S.K.; Jayabalan, R.; Sharma, N.; Bastia, A.K.; Mohanta, T.K. Antimicrobial, Antioxidant and Cytotoxic Activity of Silver Nanoparticles Synthesized by Leaf Extract of *Erythrina Suberosa* (Roxb.). *Front. Mol. Biosci.* **2017**, *4*, 14. [[CrossRef](#)] [[PubMed](#)]
50. Kora, A.J.; Arunachalam, J. Green Fabrication of Silver Nanoparticles by Gum Tragacanth (*Astragalus Gummifer*): A Dual Functional Reductant and Stabilizer. *J. Nanomater.* **2012**, *2012*, 869765. [[CrossRef](#)]
51. Gharibshahi, L.; Saion, E.; Gharibshahi, E.; Shaari, A.; Matori, K. Structural and Optical Properties of Ag Nanoparticles Synthesized by Thermal Treatment Method. *Materials* **2017**, *10*, 402. [[CrossRef](#)]
52. Xiang, F.; Zhao, Q.; Zhao, K.; Pei, H.; Tao, F. The Efficacy of Composite Essential Oils against Aflatoxigenic Fungus *Aspergillus Flavus* in Maize. *Toxins* **2020**, *12*, 562. [[CrossRef](#)]
53. Bunghez, F.; Morar, M.A.; Pop, R.M.; Romanciuc, F.; Csernatoni, F.; Fetea, F.; Diaconeasa, Z.; Socaciu, C. Comparative Phenolic Fingerprint and LC-ESI+QTOF-MS Composition of Oregano and Rosemary Hydrophilic Extracts in Relation to Their Antibacterial Effect. *Bull. Univ. Agric. Sci. Vet. Med. Cluj-Napoca. Food Sci. Technol.* **2015**, *72*, 1–8. [[CrossRef](#)]
54. Yoncheva, K.; Benbassat, N.; Zaharieva, M.M.; Dimitrova, L.; Kroumov, A.; Spasova, I.; Kovacheva, D.; Najdenski, H.M. Improvement of the Antimicrobial Activity of Oregano Oil by Encapsulation in Chitosan–Alginate Nanoparticles. *Molecules* **2021**, *26*, 7017. [[CrossRef](#)]

**Disclaimer/Publisher’s Note:** The statements, opinions and data contained in all publications are solely those of the individual author(s) and contributor(s) and not of MDPI and/or the editor(s). MDPI and/or the editor(s) disclaim responsibility for any injury to people or property resulting from any ideas, methods, instructions or products referred to in the content.